

DESIGN PROPOSAL AND WING BOX MANUFACTURING OF A SELF-LAUNCHING SOLAR-POWERED SAILPLANE

by Prof. Ing. Giulio Romeo - Politecnico di Torino
Dept. of Aerospace Eng., Turin, Italy

Presented at the XXV OSTIV Congress, Saint Auban, France

Summary

A preliminary study for a powered sailplane capable of taking-off and climbing to 500 m powered by batteries-stored (solar) energy and maintaining a level flight by taking advantage of direct sun radiation only is reported. The final configuration of HELIPLANE has a 24m rectangular wing span with two brushless motors, each one powering a propeller blade of 2 m diameter. A 13kW power would be available, during the take-off and climbing, both by 400N of nickel-cadmium rechargeable batteries as well as by the 30 m² of 17% efficiency solar cells. A T-tail configuration with a horizontal stabilizer having 6m span has been chosen. The most important structural elements are made of CFRP in order to reduce the sailplane mass. A 6 meter long wing-box has been manufactured by using a graphite/epoxy pre-preg and cured by autoclave cycles. Shear - bending- torsion tests have been carried out up to the failure load. A good correlation has been obtained between the theoretical and experimental structural results. Compression flange and sandwich panels showed a good postbuckling behaviour up to a load 25% greater than buckling load. Failure has occurred, at a bending moment

of 19 kNm, by debonding of the spar from the skin panel because of a poor bonding.

1. Introduction

Several successful projects, both sport records and scientifically oriented (Solar Challenger, Sunseeker, Icaré 2 and Pathfinder), have demonstrated that it is possible to produce a flying vehicle capable of remaining sustained in flight for long periods just thanks to the power of the sun. An accurate integration of the best standard achievable for each technological item involved is, however, necessary. Structural weight optimization, low aerodynamic drag, improvements in the lightness and efficiency of solar cells, and reliability and efficiency of electrical motors and control system are all required.

Limited levels of sun irradiation intensity are available at the usual flight altitude. The available solar radiation changes from minute-to-minute and day-to-day due to the rotation of the Earth and of the inclination of the Earth's rotational axis. The average solar radiation received at the edge of the atmosphere is 1353 W/m². By taking into account declination of the sun, latitude, solar hour angle, incidence angle, azimuth angle, atmospheric absorption,

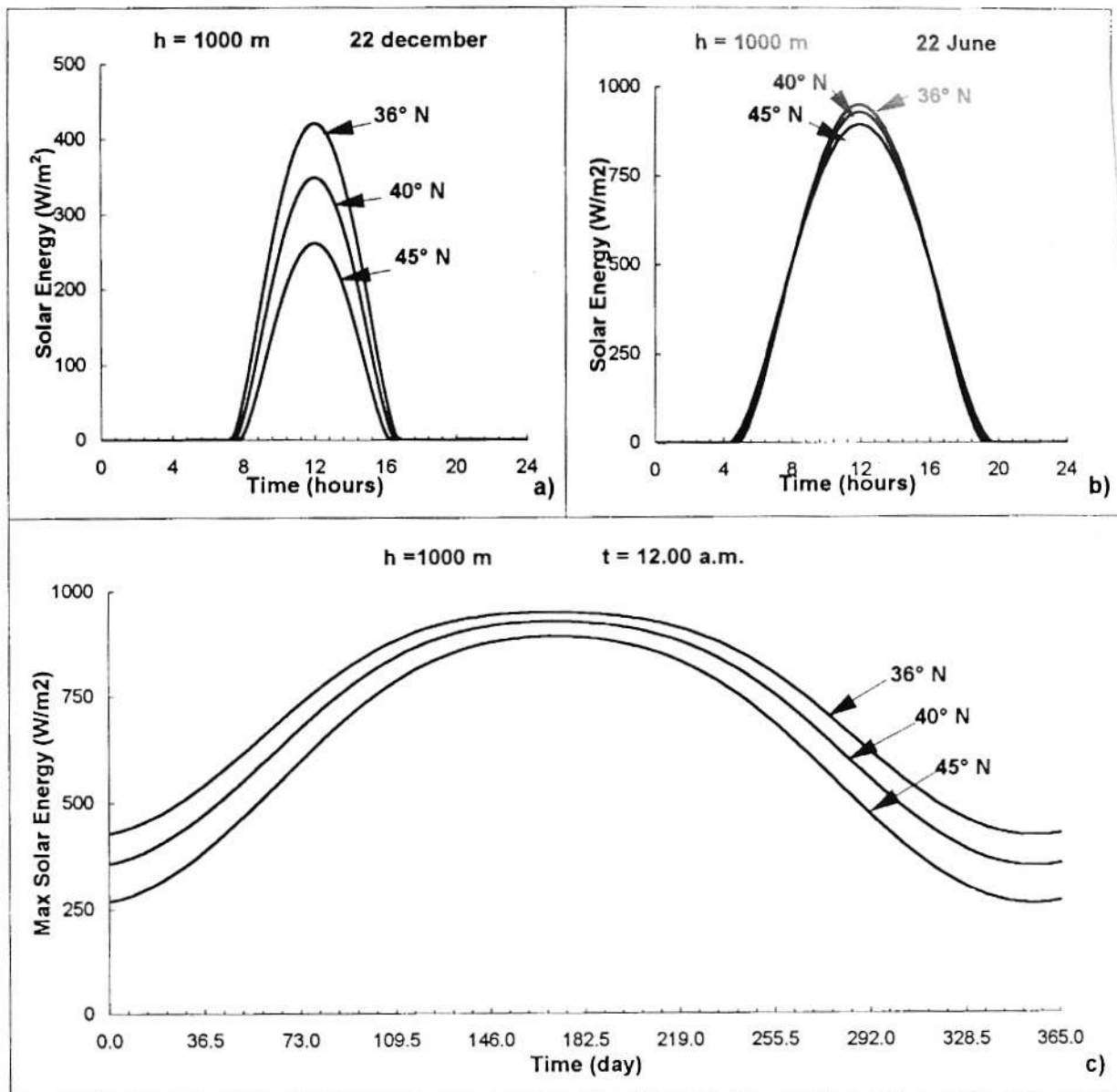


FIGURE 1. Daily and yearly solar energy distribution at several latitude.

etc. a medium to large part of the solar irradiation is lost. The typical solar energy available for a clear day at 1000 meters of altitude is reported in Figure 1. In the worst day (22 Dec), the maximum specific solar power, for a short period of time, is of $420 W/m^2$ and $260 W/m^2$, respectively, at 36° and 45° N. lat. (Figure 1a). During the best day (22 June), the maximum specific solar power for a clear day is of $950 W/m^2$ and $890 W/m^2$, respectively, at 36° and 45° N. lat. (Figure 1b); in this last case such power is available for a longer period of time. In Figure 1c, the maximum specific solar power available at noon along one year is reported. A power greater than $850 W/m^2$ would be available for more than 100 days of the year.

Low effectiveness of reasonably priced available solar cells still heavily affect the development rate of solar-powered sailplanes. Gallium arsenide solar cells have not been taken into consideration with this study because of

their high cost (about 200 \$/watt or 50000 $\$/m^2$). Thin (about 250 microns) high efficiency (15-17%) single-crystal silicon cells (at about 10\$/watt) have been, indeed, considered very useful for our purpose. Higher efficiencies (up to 23%) silicon cells have been recently developed; however, they are available at a very high price (130000 $\$/m^2$). Several technological tests were carried out in order to obtain flexible solar cell panels; by manufacturing a cell sandwich panel in which solar cells have been bonded to two thin plastic foils, by very thin transparent adhesive layers, and autoclave cured at $120^\circ C$. A good specific mass of $1 kg/m^2$ has been obtained, although we used 270 micron thick cells. Several bending tests have been carried out on cell sandwich panels giving a double curvature deflection up to 10 mm. Furthermore, CFRP sandwich panels 500 by 500 mm (with solar cell panels bonded on the surface) were subjected to a transverse distributed load

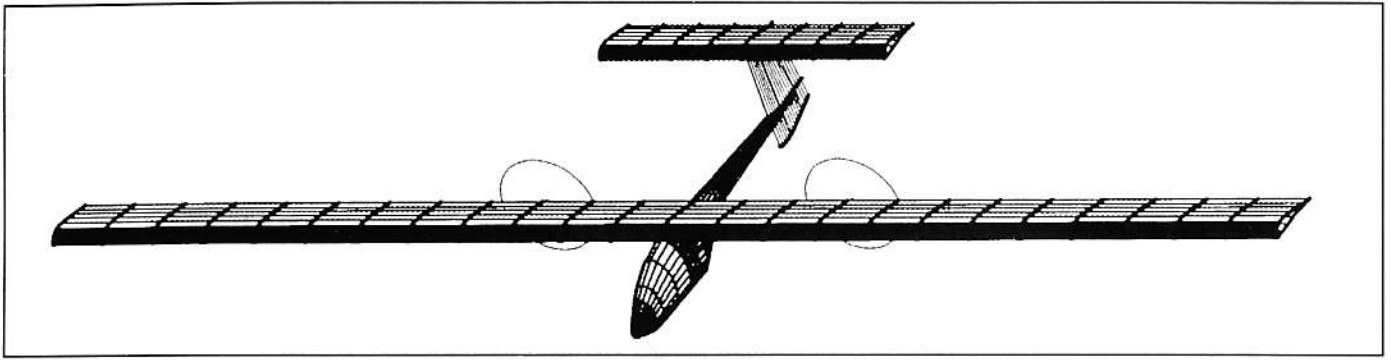


FIGURE 2. Configuration of the solar-powered sailplane HELIPLANE.

(four times the expected value). A maximum central deflection of 5 mm has been obtained, without any electrical voltage output variation of the cell. Lastly, a solar cell sandwich panel has been bonded to the wing box and tested for shear/bending. Although the wingskin was working in post-buckling field, with very high double curvature deflection, no electrical voltage output variation was recorded.

2. Design Considerations

2.1 Energy Storage and Propulsion System

An energy storage system is necessary in a solar-powered sailplane for taking off and climbing with safety up to 500 m. A minimum vertical rate of climb of 2 m/s is, in fact, required for safety reasons. By direct sun radiation, a vertical speed of only 0.5 m/s would be achievable. Rechargeable nickel-cadmium batteries have been considered for our applications due to their relatively high specific energy (up to 80 Wh/kg). The discharge-time of our batteries system has to be greater than 300 seconds. Several parameters could influence the system efficiency such as current intensity discharge, resistance due to the connections between multiple batteries, internal resistor, etc. Hundreds of tests were carried out in our University on several type of batteries, to investigate the discharge time as function of current intensity. Maintaining a quasi-uniform voltage; the discharge time is 900 s, available at 15 A, to 320 s at 40 A, with an efficiency changing from 0.99 to 0.93. Good efficiency is obtainable with a rare-Earth magnet brushless motor (94%), a low specific mass (1-1.5 kg/kW), inverter (96%) and good propeller design (88%).

2.2 Aerodynamics

A very important parameter is the coefficient of drag of the vehicle. Since limited solar energy is available, and to

minimize the power required for a horizontal flight, it is necessary to minimize the parameter C_D/C^3L^2 . We preferred to reduce coefficient of drag instead of increasing the coefficient of lift because of the greater structural load. The profile chosen for our wing is, at the moment, the Wortman FX 67-K-170. It has been chosen since all the geometrical and many experimental aerodynamic results were available. Furthermore, a very low drag profile C_{D0} was available in comparison with many updated profiles with higher coefficient of lift. This low drag is also maintained up to a good angle of attack. Of course, many new profiles give better performances, however, their geometrical data and experimental wind-tunnel results at many Reynolds numbers are not available. The wing has a rectangular planform to reduce the manufacturing cost of the very large mold for the autoclave cure of the main wing-box. At high speed, and low coefficient of lift, the wing profile drag is 60% of the total drag, the parasite drag (fuselage, interaction with wing, tails) 28% and the wing-induced drag is 12%. Indeed, at low speed, and high coefficient of lift, the wing-induced drag takes a high percentage of the total drag (about 69%); the wing profile drag is 21% of the total drag and the parasite drag 10%. Tapering and twisting the wing at least one third for each half-span would reduce the wing induced drag another 7% and a 5% reduction on the total airplane drag should be obtained, but at higher production cost. Vertical and horizontal tails do not give a high contribution to the overall drag by choosing the Wortman profile FX 71-L-150/30 or 20.

The fuselage drag and the interaction between fuselage and wing are the main parasite drag elements to be re-

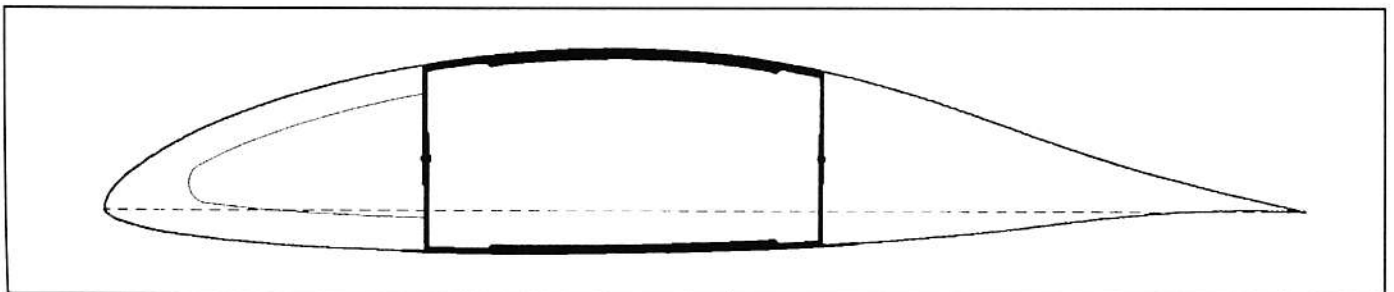


FIGURE 3. Typical wing cross-section.

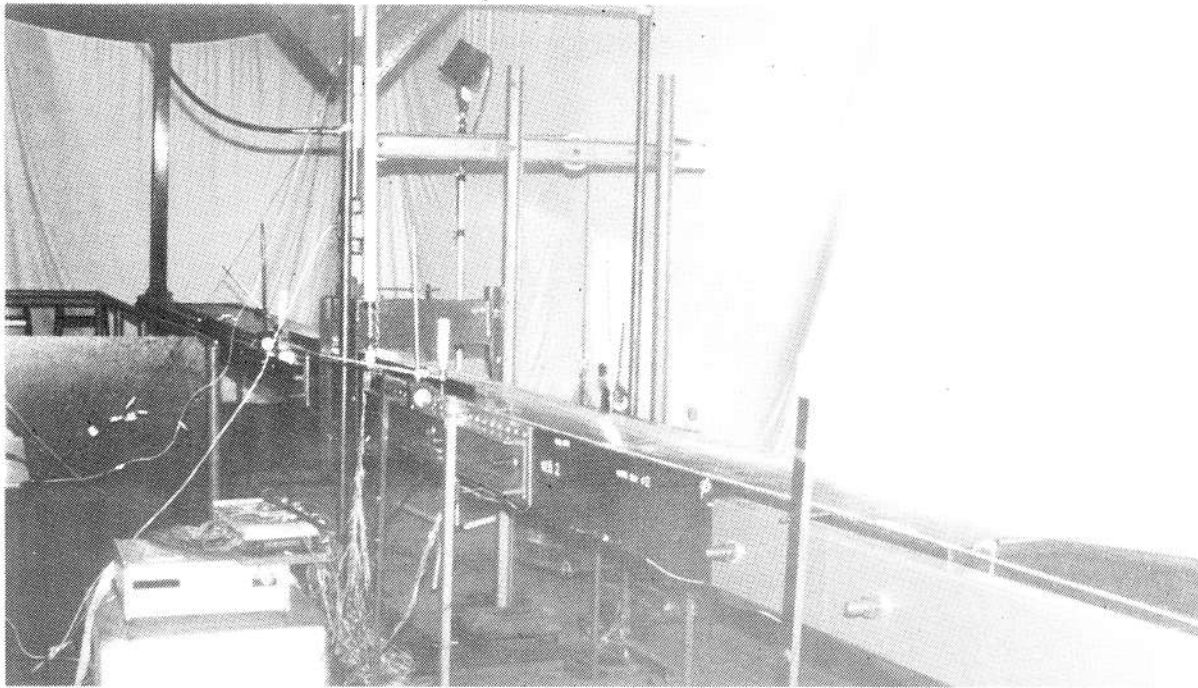


FIGURE 4. Six m long graphite/epoxy wing-box and shear-bending test equipment.

duced. Since the propeller blades (2 meters of diameter) are installed on the wing, the fuselage is not as thin up to the wing intersection and aerodynamic transition. Thereafter, the wetted surface is drastically decreased in order to reduce the friction drag. A computer program has been developed by our aerodynamic researchers in order to obtain the stream lines of the wing profile at certain angles of attack; on this basis the fuselage shape is designed. As a final result, an efficiency of 36 at 57 km/h has been calculated. With a solar energy of 1000 W/m^2 , a maximum speed of 92 km/h should be possible in horizontal flight. A 10% better performance should be possible by using a new design for the wing profile and shape. An airplane model (scaled to 1:5 and wing span limited to 2 meters) is under construction for testing in a 3m diameter wind tunnel.

2.3. Final Configuration

A first final configuration of HELIPLANE (Helios Airplane) (Figure 2) has a 24m rectangular wing span with two brushless motors, each one powering a propeller blade of 2m diameter. A total of 13kW power would be available, during the take-off and climbing to 500m, both by 400N of nickel-cadmium rechargeable batteries as well as by the 30 m^2 of 17% efficiency solar cells. A T-tail configuration with a horizontal stabilizer having 6m span and 1m chord has been chosen. The main characteristics are:

Wing Area= 28.8m^2 ; Wing span=24m; Aspect ratio=20; Power=13kW; $n=+4.5, -2.75$.

Weight=3200N (Pilot=900N; Wing=650N; Solar cells=300N; Battery=400N; Engines=250N).

$V_D=120 \text{ km/h}$; $V_{S1}=46 \text{ km/h}$; $V_{solar}=92 \text{ km/h}$ (1000 W/m^2); efficiency=36.

The airframe is about 50% of the empty mass, the solar cells 13% and the battery 18%. An improvement of 20% for solar cells efficiency would produce a 20% reduction of the

dimensions or would give a greater power.

3. Manufacturing Problems

The 24m wing and the 6m horizontal stabilizer will be manufactured within the next year to show the strength and stiffness of such very light airplane structure. The main wing box structure (two C-spar and two skin sandwich panels) will be manufactured in three pieces (8m long each) by using a graphite/epoxy M40J/919 pre-preg tape (grade 145, 37% resin weight) cured by an autoclave cycle at a temperature of 120°C . The main lamina mechanical properties are:

$E_1 = 220\text{GPa}$; $\sigma_1 = 2000\text{MPa}$; $\delta_1 = 1.2\%$; $\rho = 1.65\text{kg/dm}^3$.

After curing, lower and upper panels are bonded to the ribs and riveted along the neutral axis of the webs co-cured with each panel (Figure 3), to form 3 boxes. Then the three parts are joined by two bolts for each side in the half meter of overlapping between two adjacent wing-boxes. Leading and trailing edges are manufactured of foam and bonded to the wing box. A computer program has been developed for designing the anisotropic wing box, under shear-bending-torsion load, in order to choose the proper lay-up and thicknesses that would minimize the wing mass, leading to a maximum tip deflection of 1.5m and angle of twist of 2 degrees. A particular design has been developed for manufacturing the fuselage. A very-light pin-jointed CFRP truss-structure is being manufactured to carry the applied load. CFRP tubes are bonded one to each other, by adhesive joints, to form up to seven connections. Thin layers of glass fibers would be modelled around foam to obtain the aerodynamic shape. The horizontal stabilizer is manufactured by a multi-ribs structure; a main tubular sandwich spar, having CFRP faces and Nomex core, that will sustain all shear, bending, and torsion load. A secondary small tubular spar will also be used to support the elevator.

Additionally, 12 ribs will connect the two spars as well as will support 6 mm thick rigid PMI upper panels where the solar cells would be bonded. A technological demonstrator, 1.3 m long, was manufactured for getting experience with the production. The tubular spar was manufactured by using a graphite/epoxy prepreg and cured at 170 °C. Several shear - bending - torsion tests have been carried out to obtain a very good correlation between theoretical and experimental results [1].

4. Experimental Tests

A 6 meter long wing-box has been manufactured for gaining experience with a very long structure. T-300 graphite/epoxy pre-preg, having about half the mechanical properties of the M40J fibers, has been used and cured by autoclave cycles at 180 °C. For simplifying the production, the main and secondary C spars were cured separately from upper and lower sandwich panels; after which the main C spar was bonded (at room temperature) to the two panels by applying a proper pressure both from inner and

outer sides. Then secondary spar and ribs were bonded all together by applying outer pressure only. Since a 2.2 m maximum autoclave length was available in our laboratories, the wing box was manufactured in three pieces and joined together by 4 bolts for each side (Figure 4). The following principal dimensions have been obtained.

Spar Flange: width =75 mm; lay-up = $(\pm 45/0_2/\pm 45/0)_2$; thickness =3.9 mm.

Sandwich panel: width =505 mm; lay-up = $(\pm 45_2/Nomex)_S$; face =0.4 mm; core =6 mm; mass = 2kg.

Rib: width =490 mm; lay-up = $(\pm 45/0-90/Nomex)_S$; face =0.4 mm; core =6 mm; mass =0.125 kg.

Spar webs have different lay-up and thickness, up to 4 mm, depending from the fitting.

Special equipment has been developed to carry out the shear - bending - torsion test (Figure 4). A one meter steel frame has been bolted to each wing box end for applying the limit load in the root section and the ultimate load in the fitting section between two boxes. The steel frame has been

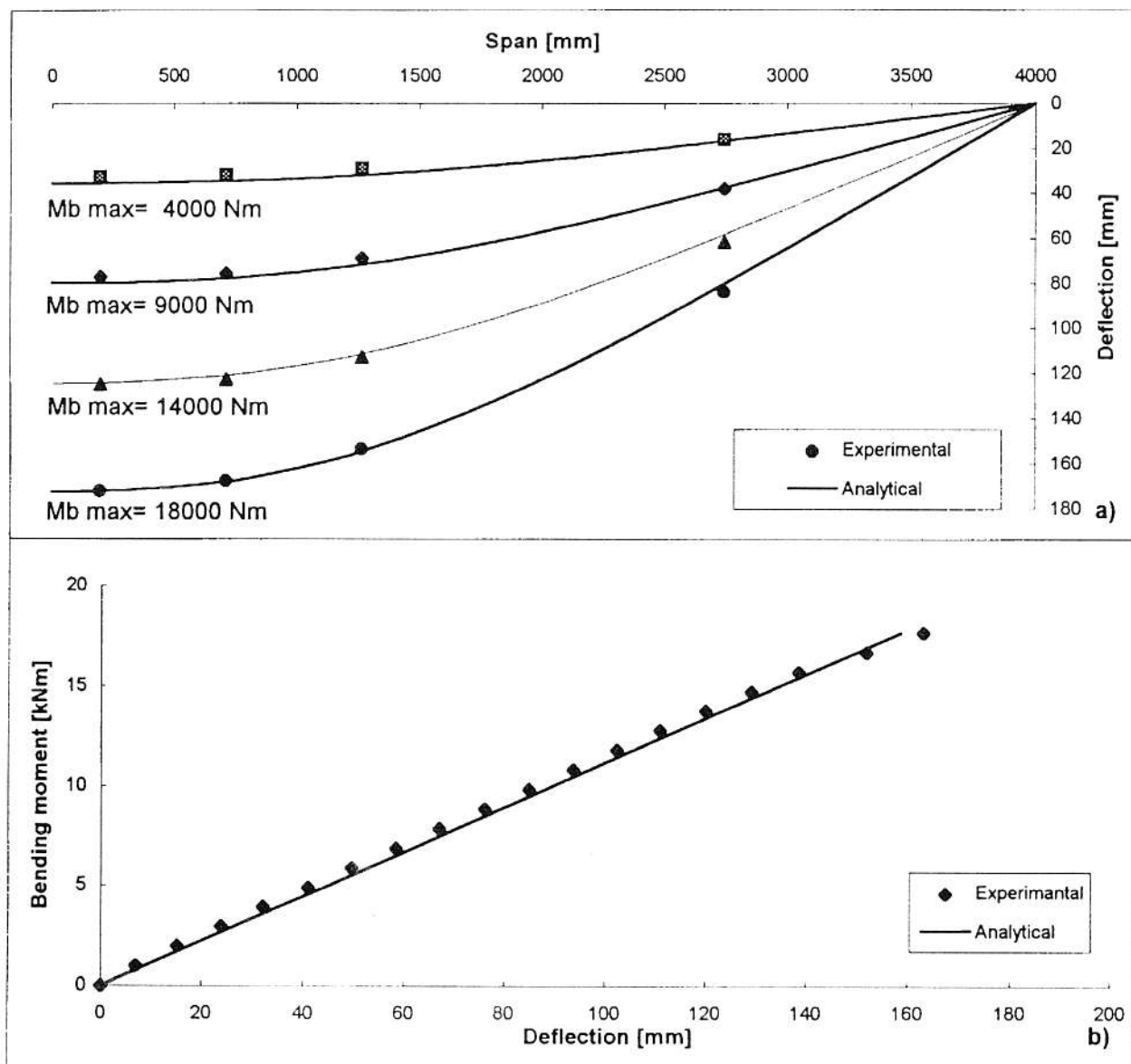


FIGURE 5. Deflection as function of bending moment. Comparison between analytical and experimental results.

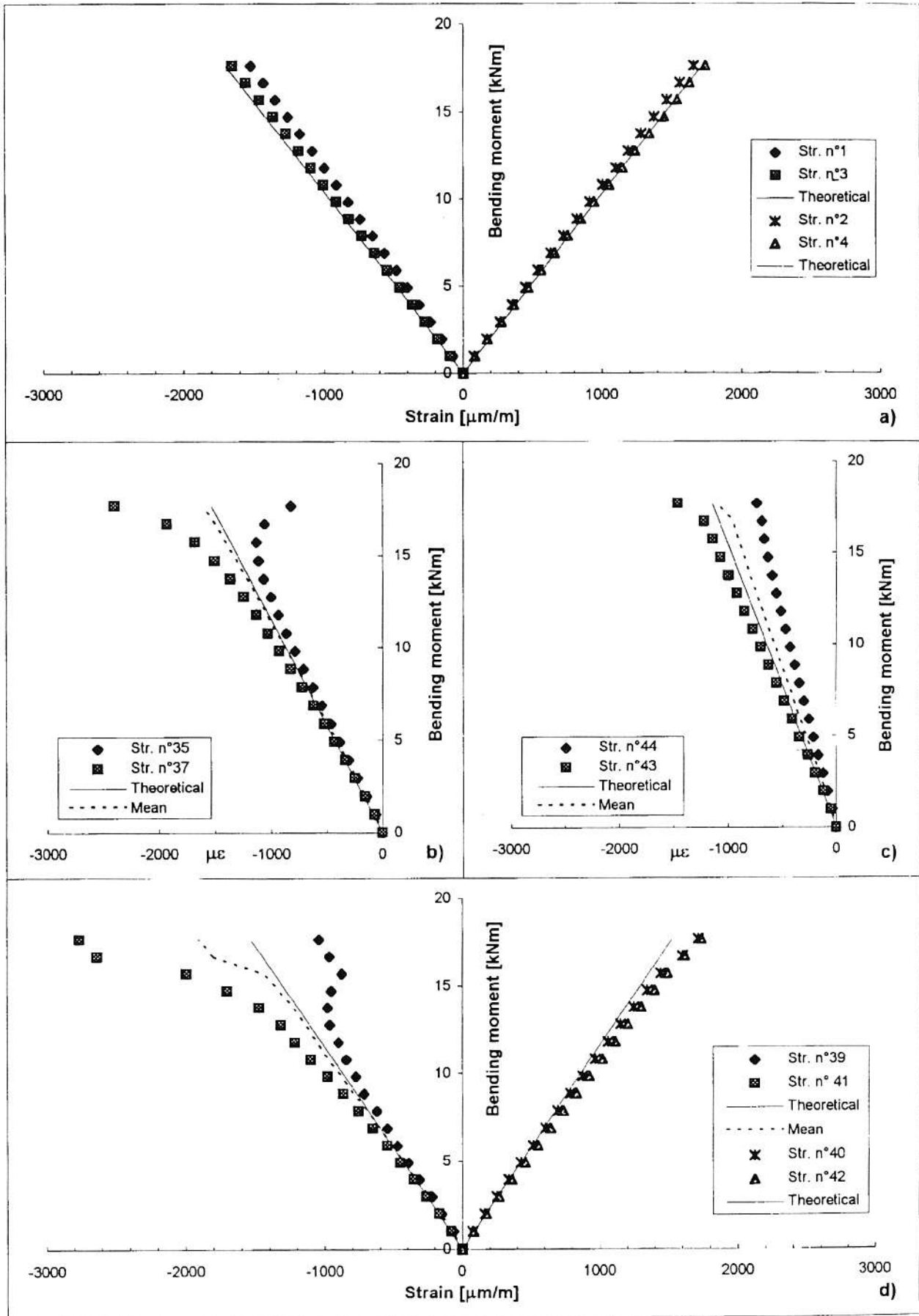


FIGURE 6. Comparison between analytical and experimental strain results of shear-bending test.

hinged to the roof. The load is applied in the root section, by a hydraulic jack, step-by-step. In the first tests, the load has been applied in the wing-box shear center. In order to carry a shear-bending test, 56 strain-gauges were bonded, (when possible, back-to-back) to several parts of the wing-box. Deflections were measured along the span.

4.1. Shear-bending test and torsion test

Several experimental and analytical results are reported in Figure 5. The deflection along the span is first drawn in Figure 5a, for several values of the maximum bending Moment (M_b max) applied in the root section. A good correlation has been obtained between the theoretical and experimental results by taking into account the rotation between the inner and outer wing-boxes. The correlation is clear (Figure 5a) at 1 m from the root section. The deflection measured at 210 mm from the root section as a function of the maximum applied bending moment is reported in Figure 5b. Almost linear behavior was recorded up to the buckling load of upper spar (about 15 kNm), where the deflection rate increased. The buckling behaviour of the upper spar is very clear from Figures 6 and 7. Back-to-back strains, measured in the main spar at 2 meters from the root section, are reported in Figure 6b (Str. gauges n.35-37) for the left section and Figure 6d (Str. gauges n.39-41) for the right section. A strain reversal occurred showing halfwave

buckling. As a consequence, the lower spar flange (gauges n.40-42) has been overloaded. The rotation of the upper panel (due to the eccentricity of the applied load) is shown by the different strain values recorded, (note back-to-back gauges n.44 and 43 Figure 6c). In the root section (Figure 6a) (where spar was reinforced) no buckling occurred as can be seen from gauges n.1-3, placed in the upper flange, and n.2-4 in the lower flange.

Failure has occurred, at a bending moment of 19 kNm, by debonding of the left outer wing-box spar from the skin panel (Figure 7). This was caused by an erroneous use of liquid release agent in manufacturing one spar. Normally solid FEP release agent was used on the steel mold before laying-up the pre-preg in order to easily remove panels after the autoclave cure cycle. However, for one spar production we used a liquid release agent sprayed on the steel mold. This agent perhaps contaminated the CFRP spar during the cure cycle. Although good bonding seemed to happen (as checked by an ultrasonic thickness control) bonding has shown to be very weak. The outer wing-box spar buckled, and high peel stress arose in the adhesive layer. The panel also disbonded from the spar. By visual observation, no trace of adhesive was seen on the spar and it is clear that adhesive didn't adhere to the spar where liquid the release agent was used. Nevertheless, a load 10%

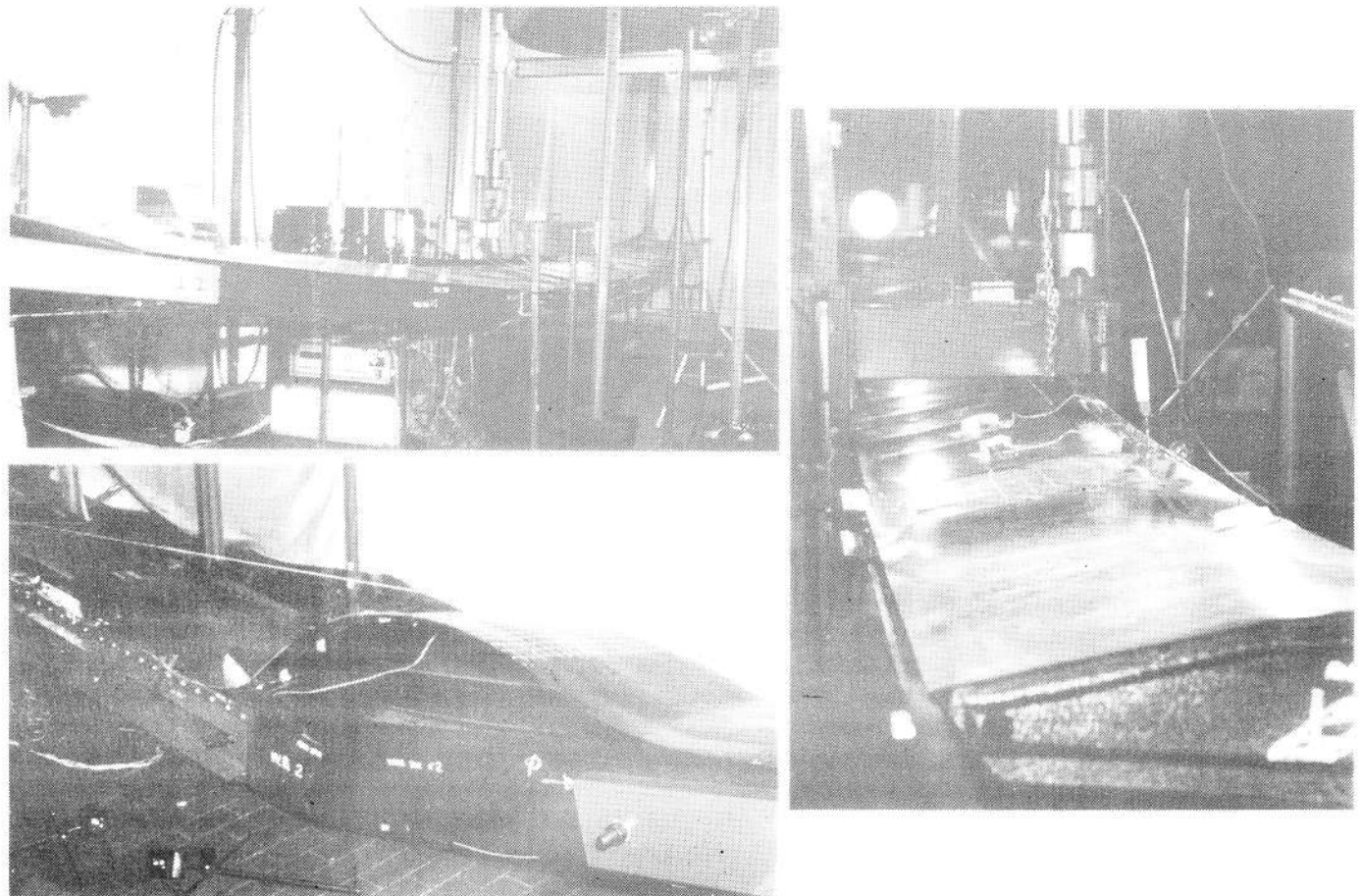


FIGURE 7. Deflection buckling and failure of the wing-box under shear-bending test.

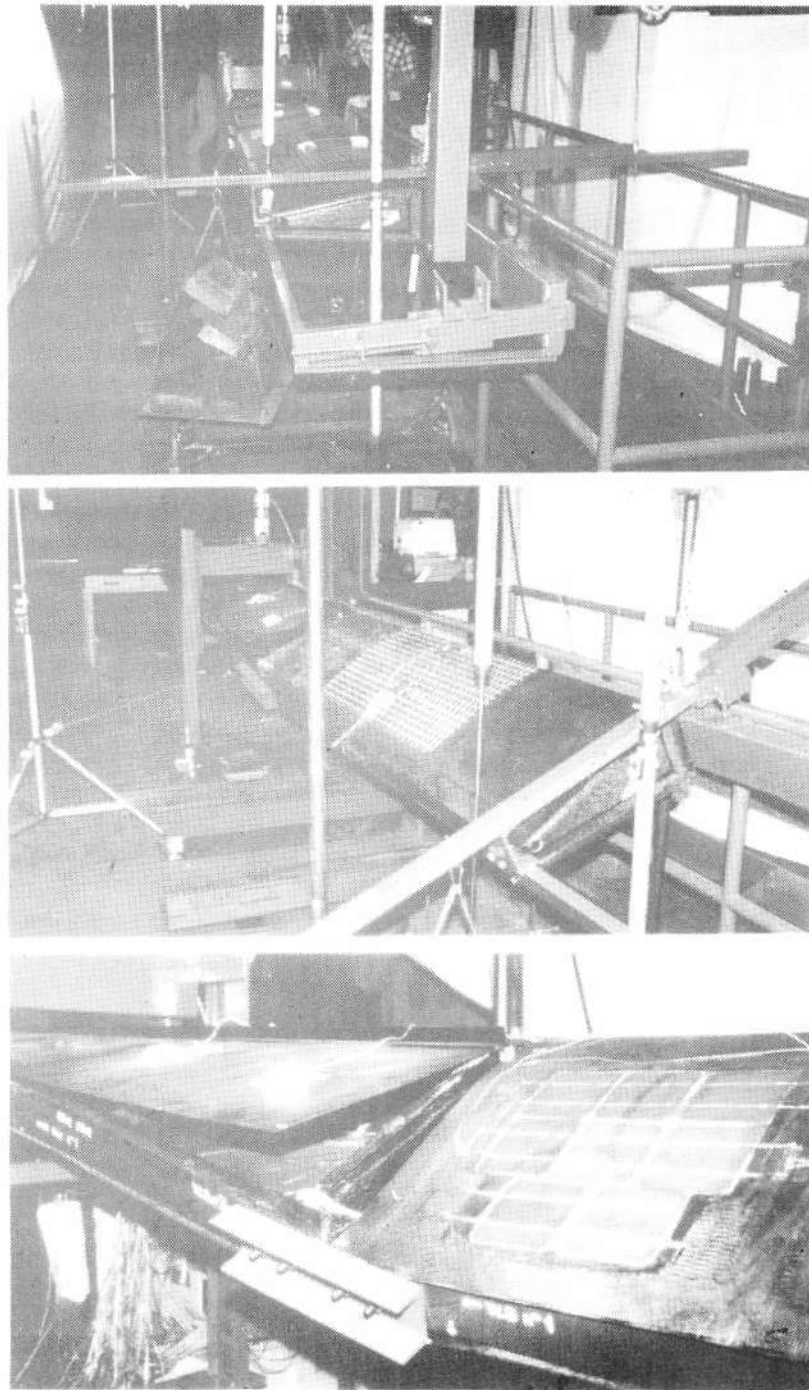


FIGURE 8. Test equipment and failure of the wing-box under pure torsion.

lower than the limit load was reached in the root section and the ultimate load reached in the fittings.

Since only the left outer wing-box was broken, torsion tests have been carried on the remaining three meters long wing-box. With the root section clamped, a pure torsion load was applied on the box end (Figure 8). The angle of twist along the span is plotted in Figure 9a at the limit torsion moment of 705 Nm. A sharp twist gradient was recorded at 1 m from the root section, because of a 5 mm gap between inner and outer boxes and where the C-section beam was providing all the torsion rigidity. This

effect will not be present in the final flight structure. The angle of twist as a function of the applied torsion moment is reported in Figure 9b for two sections. An almost linear behavior was recorded up to three times the limit load and good correlation has been obtained between the theoretical and experimental results taking into account the twist gradient between the inner and outer wing-boxes. The shear strains in the main spar web is finally reported in Figure 9c. Failure has occurred, at a torsion moment of 2.1 kNm, by debonding the central wing-box skin panel from the rear spar at an applied load of 3 times the limit load

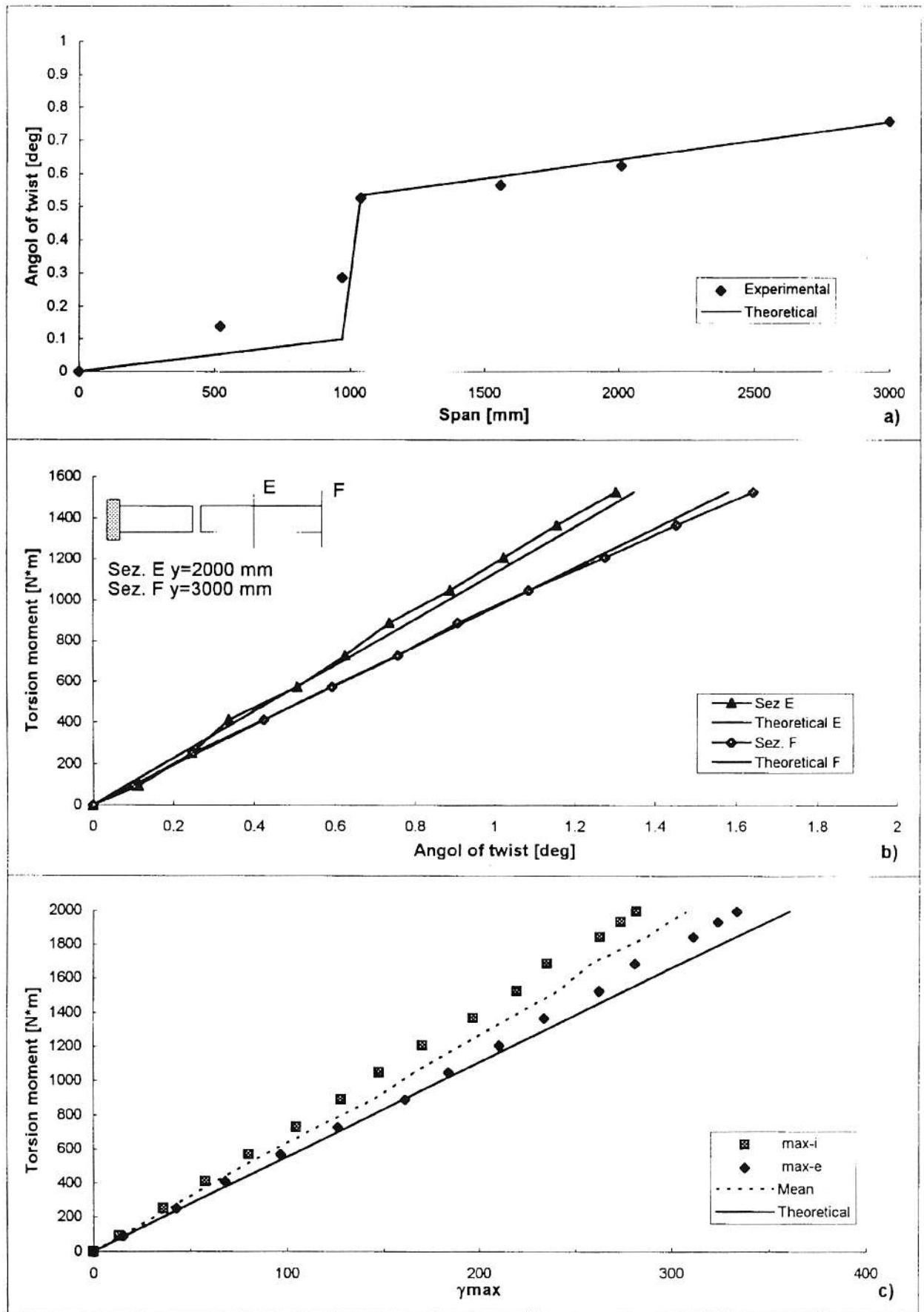


FIGURE 9. Angle of twist and web shear strain as function of torsion moment. Comparison between analytical and experimental results.

(Figure 8).

Conclusion

Ten advanced composite panels or wing boxes, less than 1 m long, were manufactured in the last 15 years by autoclave cure in the composite laboratory used by our students and by myself. This was the first time that an advanced composite wing-box 6 meters long was manufactured in an Italian aeronautical engineering University.

Several lessons were learned from the experimental tests.

- a) The bearing stress of CFRP joints is very much affected, not only by the panel lay-up as was very well known, but also by the use of fabric instead of tape material; from the many tensile tests carried-out on specimens made by UD layers oriented at $(\pm 45/0_6/90_3)_S$ where a bearing stress of 450 MPa was obtained. In manufacturing the spar-webs, it was easier to use fabric layers oriented with the lay-up $(\pm 45/0-90_2)_{2S}$. The bearing stress was reduced at 300 MPa with this lay up. A higher reduction was recorded for the shear-out stress from 94 MPa in UD specimens to 44 MPa in fabric specimens. This may be the reason for the fitting failure of the first test at a bending moment of 12 kNm.
- b) After reinforcing the spar webs with a thin steel plate, the test has been repeated up to the failure load. At a bending moment of 15.5 kNm the spar flange started to buckle. The buckling load of the flange (considered as simply supported on four sides) should be at a much higher load, as predicted by our analysis and very well confirmed by many tests of biaxial compression and shear combined loads carried on panels dimensioned at 1000 by 700 mm. The reason for this variance in

advance buckling behavior is due to the large gap (about 40 mm) between spars or ribs and the effective sandwich panel. Bonding of the skin panels to both sides must be made by the face layers only (0.8 mm thick), since the honeycomb must be tapered. When the compression load, as well as the crushing load due to bending curvature, is applied to the upper panel an eccentric load arises on this thin skin generating a rotation of the upper sandwich panel. As a consequence, one side of the flange is not supported by the sandwich panel and buckles at a load much lower, thereby inducing a very high deflection in the skin. To avoid a large deflection of the solar cells the flange and upper skin have been designed not to work in the post-buckling field, at least up to the limit load. Although we learned to avoid the above problem, we have showed that sandwich panels with bonded solar cells can work at high deflection, and with double curvature, up to a load 25% greater than buckling load.

The many lessons learned, from technology as well as from testing, have given us several good implementations for the final design of the motorglider. Manufacturing has been started and we hope it will fly prior to the next OSTIV Congress.

Acknowledgments

The authors acknowledge the efficacious cooperation of F. Brunello, L. Carano, G. Frulla, P. Marzocca and A. Oddenino.

References

1. Romeo G., Frulla G.: "Analysis of a Composite Material Wing Structure for a Solar Energy Airplane." Proc. XIII AIDAA Nat. Congress, Roma, Sept. 1995, Vol. II, pp. 965-976. (In Italian).